Australian Earthquake Engineering Society
2024 National Conference, 21-23 November 2024
Adelaide, South Australia

Earthquake Environmental Effects during the 2021 Mw 5.9 Woods Point Earthquake, Southeast Australia: Evidence for low shaking intensity in the epicentral region?

James La Greca[1], Mark Quigley[1], Yuxiang Tang[1]

1. School of Geography, Earth, and Atmospheric Science, The University of Melbourne, Parkville, Australia

Corresponding Author: James La Greca (james.lagreca@student.unimelb.edu.au)

Abstract

Instrumental records of near-source seismic ground motions (i.e., within a few kms of fault ruptures) are sparse. Understanding near-source ground motion intensity distributions (e.g., peak ground accelerations and velocities) is important for evaluating seismic hazards to people and infrastructure proximal to active faults. The 2021 M_w 5.9 Woods Point (WP) earthquake produced a suite of Earthquake Environmental Effects (EEEs) in the epicentral region (i.e., <50 km) that we evaluate using the Environmental Seismic Intensity Scale (ESI-07). We compare ESI-07 estimations to ground shaking intensity predictions from ground motion models (GMMs). ESI-07 estimates within 5 km of the surface projection of the WP earthquake source fault are lower than anticipated from GMMs. We hypothesise that the source characteristics of the WP earthquake (bilateral strike-slip faulting on a steep, blind fault) resulted in lower-intensity shaking at spectral periods relevant for EEEs in the epicentral region, and that this damping effect diminished at increasing distances from the fault, where ESI-07 estimates of shaking intensity increase. Possible contributions from directivity effects, topographic factors, and sampling biases may also be relevant. Further studies of near-fault ground motions (e.g., physics-based simulations) are required to evaluate this hypothesis, which has important implications for GMMs.

Keywords: Earthquake environmental effects, ground motion, seismic hazard, source characteristics

1 Introduction

Strong ground motions resulting from earthquakes are often anisotropic, with ruptures producing immediate near-source ground motions strongly influenced by rupture directivity and/or elastic rebound (i.e., fling) effects (Aagard et al., 2004; Dreger et al., 2011; Hisada and Tanaka, 2021; Luo et al., 2020). This variability in strong ground motion has significant implications for probabilistic seismic hazard analyses (PSHA), particularly concerning whether ground motion models (GMMs) accurately represent anticipated near-field ground shaking levels. Numerous studies have attempted to classify and quantify the effects of directivity, fling, and radiation patterns on ground motions (e.g., Sommerville et al., 1997; Kotha et al., 2019; Luo et al., 2020; Hisada and Tanaka, 2020; Dreger et al., 2011; Aagard et al., 2004). These studies use a combination of physics-based modelling (for when there is difficulty obtaining near-source ground motion), while some of the studies (Kotha et al., 2019; Somerville et al., 1997) use empirical data from regions with high seismic network density.

Obtaining direct observations of instrumentally recorded ground motion intensities has been difficult due to lack near-source instrumentation. Efforts have been made to obtain near-source recordings of earthquakes by emplacing accelerometers and strong motion seismometers near faults with high recurrence rates (e.g., San Andreas, Parkfield Rupture), but issues such as data clipping, and lack of dense coverage (including azimuthal coverage) continues to be an issue. These challenges are even more pronounced in stable continental regions (SCRs), where moderate to large magnitude earthquakes have lower recurrence rates, providing fewer opportunities to record events. Additionally, SCRs often have less dense seismic networks than more active regions. Alternative methods including macroseismic intensity scales have been developed to obtain seismic intensity measurements namely, the Modified Mercalli Intensity scale (MMI; Wood and Neumann, 1931) and Environmental Seismic Intensity Scale (ESI-07; Michetti et al., 2007). These intensity scales are particularly useful in the absence of instrumental recordings, relying on human interpretations of shaking intensities (MMI) and on observed environmental effects (ESI-07).

In this study, we document and analyse EEEs resultant from the M_w 5.9 2021 Woods Point (WP) earthquake, in southeast Australia. This earthquake occurred in a relatively sparse region of the Victorian Highlands (Figure 1), with the nearest seismometer recording than wasn't *'clipped'* more than 50km away from the epicentre (La Greca et al., 2024; Mousavi et al., 2023; Hoult et al., 2021; Tang and Mai, 2024). Recorded MMI measurements within the epicentral region were also sparse (La Greca et al., 2024). We therefore utilised the ESI-07 scale to quantify the macroseismic intensity of EEEs to understand the distribution of ground motion in the near-source region.

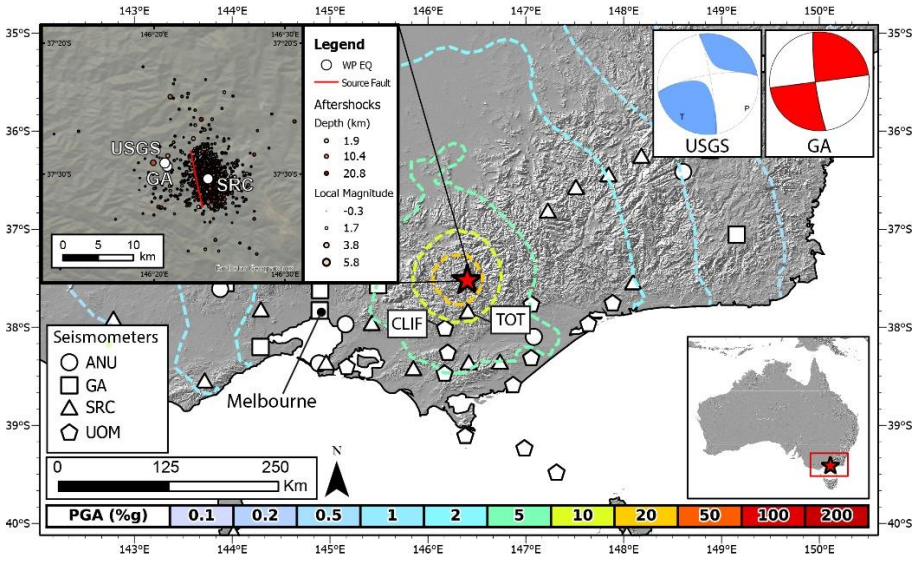

Figure 1: Map of the M_w 5.9 Woods Point earthquake in southeast Australia. USGS and GA moment tensors and present, with the distribution of the available seismic network at time of the event. Figure taken from La Greca et al., 2024. Aftershock dates range from 21/09/2021 to 19/6/2022 UTC.

2 Methodology

2.1 Data Collection

A reconnaissance field survey of environmental damage was conducted in response to the WP earthquake (Quigley and La Greca, 2021; La Greca and Quigley, 2021). Our field reconnaissance team reached the epicentral region approximately 30 hours after the earthquake. This first response took place over five consecutive days from the 23rd to the 27th of September 2021. A second field response took place two weeks after the earthquake from the 8th to the 10th of October 2021. A third response was undertaken from the 23rd of October to the 26th of October 2021. The field response took place to investigate the epicentral region for a surface rupture, environmental damage, and infrastructure damage. All surveyed localities were assigned a geographic point-based phone and iPad GPS, with most localities photographed and paired with observational notes. Drone surveys, and iPad LiDAR imagery was used to document rock falls, road cracks, and vegetation damage. The region is hard to access due to its mountainous terrain, which resulted in observations being constrained to areas where there was direct road or track access.

2.2 Application of the ESI-07 Scale

The ESI-07 intensity scale is a macroseismic intensity tool that is used to classify the intensity of EEEs (Michetti et al., 2007; Serva, 2019; Ferrario et al., 2022). It is intended to be used with other macroseismic intensity scales, particularly if there are no other observations possible (i.e., low population density, as is the case with the WP earthquake). Michetti et al. (2007) outlines primary (e.g., surface ruptures, permanent uplift), and secondary EEEs. The study outlines the extent, distribution and amount of damage posed by the EEE as a methodology of calculating the intensity of shaking at that location. For example, "*Thin cracks (millimetre-wide and several cms up to 1 meter long) are locally seen where lithology (e.g., loose alluvial deposits, saturated soils) and/or morphology (slopes or ridge crests) are most prone to this phenomenon*" would be rated an intensity of V (5). We assess every observed EEE resultant from the WP earthquake and classify them in accordance with the ESI-07 intensity scale outlined in Michetti et al. (2007).

2.3 Ground Motion Modelling

Peak ground velocities (PGV) were calculated at the location of each observed EEE using the Somerville et al., 2009 GMM (SGC09). This GMM is selected because it matches the instrumental recordings better than other alternative models (Tang and Mai, 2023). Distances to the epicentre (R_{epi}), rupture plane (R_{rup}) and surface projection of the rupture plane (R_{jb}) were calculated using GMSS2.0 (Tang, 2022a, b) and the inputs are outlined in Table 1.

Table 1. Inputs for GMMs

Input Type	Input Value	Source
Hypocenter Latitude	-37.506	Seismology Research Center – (Quigley et al., 2021)
Hypocenter Longitude	146.402	Seismology Research Center – (Quigley et al., 2021)
Hypocenter Depth	12.7 km	Seismology Research Center – (Quigley et al., 2021)
Rake	0 Degrees	Geosecience Australia
Vs30	760 m/s	-
Rupture Plane Strike	Strike: 352.81° ± 3.2	Huang et al., 2024
Rupture Plane Dip and Dip Direction	Dip: 85.50° E ± 2.97	Huang et al., 2024
Rupture Length	4.8 - 6.6 km: Mean = 5.69 km	Huang et al., 2024
Rupture Width	6.77 - 9.31 km: Mean = 7.55 km	Huang et al., 2024

As this study evaluates observed EEEs with ESI-07, we plan to compare observed values with empirical relationships. ESI-07 is intended to be consistent with MMI. Therefore, we calculate MMI values for each EEE using PGVs that were scaled to MMI using empirical scaling relationships outlined in Atkinson and Kaka, 2007 (Equation 1).

$$MMI(PGV) = \begin{cases} 4.37 + 1.32 * \log 10\,(PGV), \text{if } \log10(\text{PGV}) \leq 0.48 \\ 3.54 + 3.03 * \log 10\,(PGV), \text{if } \log10(\text{PGV}) \geq 0.48 \end{cases} \quad \text{(eq. 1)}$$

We then construct the attenuation function for ESI-07 EEEs. Firstly, we bin the ESI-07 values through two methods: i) logarithmic bins of R_{jb} (this was to account for the wide range of epicentral distances and ensure that significant variations in intensity that often occur at smaller distances are captures and that far-field data is adequately represented), and ii) 5km spaced bins to divide the data into equal-sized intervals (this was to interpret changes in intensity over consistent distances). We fit the binned ESI-07 data to a logarithmic decay function (equation 2) and use a non-linear least squares regression to fit the parameters of equation 2 (equation 3). To mitigate the issues of sampling bias, we exclude all data points where ESI was recorded as zero. This is due to the infeasibility of documenting all locations without observed environmental damage and could disproportionately influence the analysis towards negligible intensities.

$$ESI(Rjb) = a - b \cdot \log_{10} R_{jb} \quad \text{(eq. 2)}$$

$$\min_{a,b} \sum_{i=1}^{numBins} (\text{binnedESI}_i - (a - b \cdot \log_{10}(\text{binCenters})))^2 \quad \text{(eq. 3)}$$

3 Results

3.1 Overview of observed EEEs

This study documents 171 EEEs with a R_{jb} distance ranging from 0 to 88 km (Figure 2). ESI-07 values attributed to the EEEs, ranging from locations that have no damage, up to an ESI-07 value of 7. We observe a range of EEEs such as ground cracking, tree falls, landslides, toppling failure of rock faces, and hydrological changes. All EEEs presented herein are inferred to be coseismic. We do not find evidence for a surface rupture. Several localities exhibited toppling failure up to 30 km from the epicentre. The distribution of toppling failure (i.e., percentage of a rock face surface area that has been displaced) varied, with some localities observing less than 1% failure of their overall surface area up to greater than 20% toppling failure of surface area. Coseismic extensional cracking was observed predominantly along sections of road up to ~42 km away from the epicentre. Cracking was found in both gravel and paved roads, ranging from a few mm to 5 cm. The maximum length of observed cracking was ~200 m. Damage to vegetation - specifically trees - was observed up to ~30 km from the epicentre. Most localities exhibiting damage to vegetation represented a single isolated tree fall, while some locations showed multiple (i.e., 3 – 10) trees fallen within a confined region. One location was documented as evidence for hydrological changes, with an increase in water discharge from a spring reported by a local resident. Multiple locations had document coseismic landslides, these landslides were estimated to have volume of a few hundred meters^3, with the landslide that distributed the Licola-Jamieson Road having a surface area of 460 m^2.

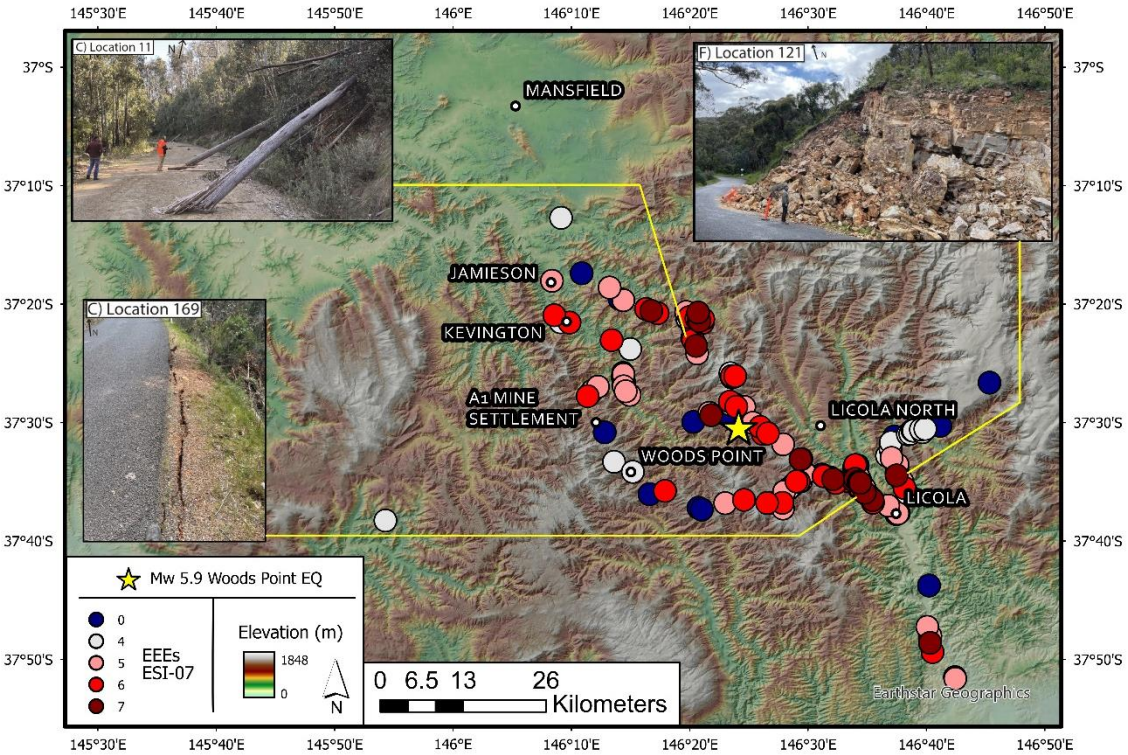

Figure 2: Map of all observed EEEs within the Woods Point epicentral region. Woods Point epicentre (yellow star). ESI-07 Values of all EEEs range from 0 (blue) to 7 (Red). There are also three examples of EEEs, Location 121 is rock fall/toppling failure, Location 169 is cm wide ground cracks and Location 11 is tree falls.

3.2 Evidence for absence of environmental damage within the immediate epicentral region

In addition to finding EEEs within the epicentral region, this study documented locations which displayed evidence for very minimal or no environmental damage (Figure 3). The basis for this data collection was the presumption that certain localities (i.e., proximity to epicentre and/or surface projection of the fault trace) should exhibit evidence for relatively high macroseismic intensity. This data can be impacted by sampling bias, particularly with the issue of azimuthal coverage. In addition to this, environmental damage can be frequency dependent which this study does not account for. We document locations that have rock faces that display no evidence (or very minor evidence - <<1% toppling failure by area) of damage, while similar rock faces with similar geological properties (i.e., slope angle and lithology) at greater epicentral distances would have far greater distribution of damage. This includes locations where precarious rocks which would have been expected to fail during seismic loading, did not.

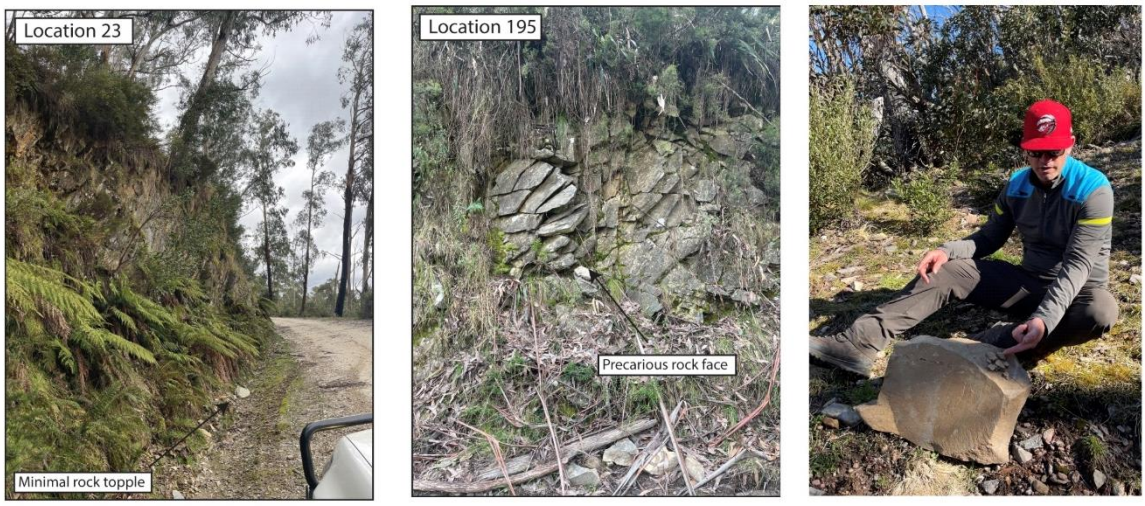

Figure 3: Locations proximate to the epicenter showing evidence for minimal to no environmental damage.

3.3 Attenuation and Distribution of Damage

The attenuation of the binned mean ESI values for both the log bin and 5 km equally spaced bin shows evidence for mean ESI values to be ~2.5 macroseismic intensity units lower than modelled MMI from the SGC09 GMM (Figure 4) based on the correlation between MMI and PGV proposed by Atkinson and Kaka (2007). When considering logarithmic bins (i.e., bins that increase in density towards Rjb of 0), we find that there is a potential decrease in shaking intensity. We find that there is not a substantial rate of decay from the near-source epicentral region to distances of 90 km.

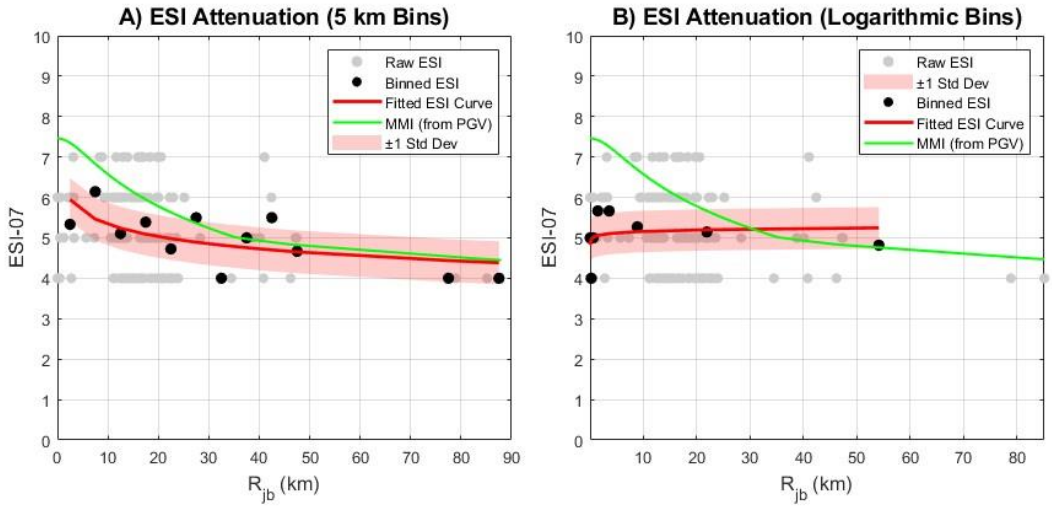

Figure 4: Attenuation of ESI-07 EEEs with R_{jb} distance. A) Attenuation using evenly spaced 5km bins. B) Attenuation using logarithmic bin sizes (i.e., High density of bins towards 0 with decreasing density with increasing distance). ESI curve (red) is a logarithmic decay function fit via least squares method of the binned mean ESI values. Green line is theoretical SGC09 GMM converted to MMI using Atkinson and Kaka, 2007 scaling relationship.

We also compared recorded ESI-07 with recorded *Did You Feel It?* (DYFI) reports collated by Geoscience Australia (La Greca et al., 2023) (Figure 5). The maximum recorded DYFI MMI is averaged at just over 7 (VII); this is consistent with the maximum recorded ESI-07 data at 7, even at small epicentral distances. Near-source MMI DYFI reports are sparse (Figure 6), and data points are often constrained by only one response. This results in difficulties in comparing ESI-07 and observed MMI for the Woods Point earthquake, but interpolated regressions may suggest that ESI-07 points to lower intensities than those derived from MMI within the near-source (<20km) epicentral region. There does appear to be a regional azimuthal N-S amplification of MMI which may be expected to be present within the near source region (Figure 6).

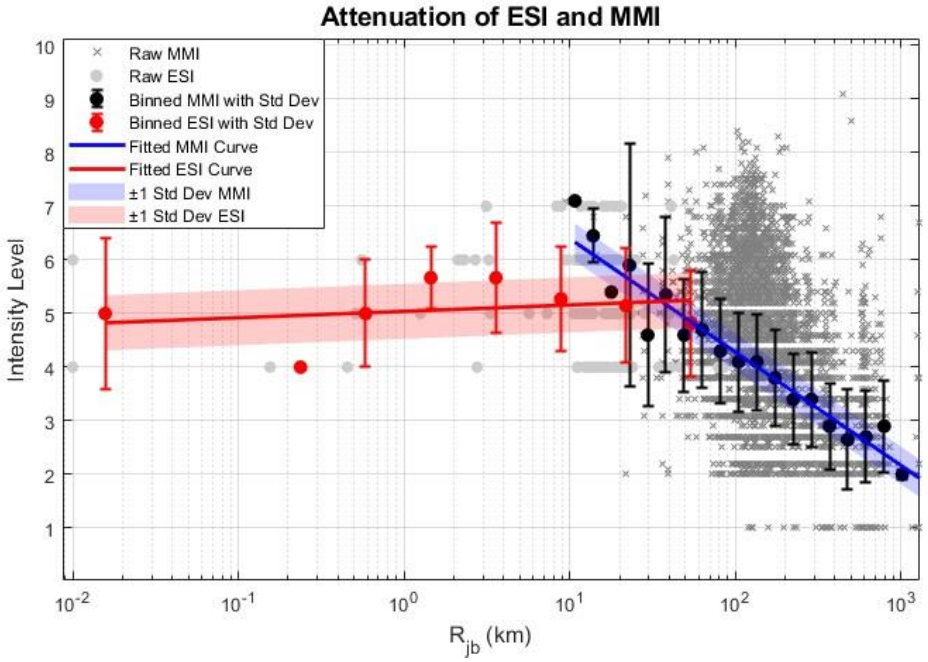

Figure 5: Modified from La Greca et al., 2024. Grey Dots are ESI-07 Data presented in this study compared against MMI data (grey crosses) from raw Did You Feel it? Reports (DYFI) felt reports and black circles are binned MMI from the DYFI reports.

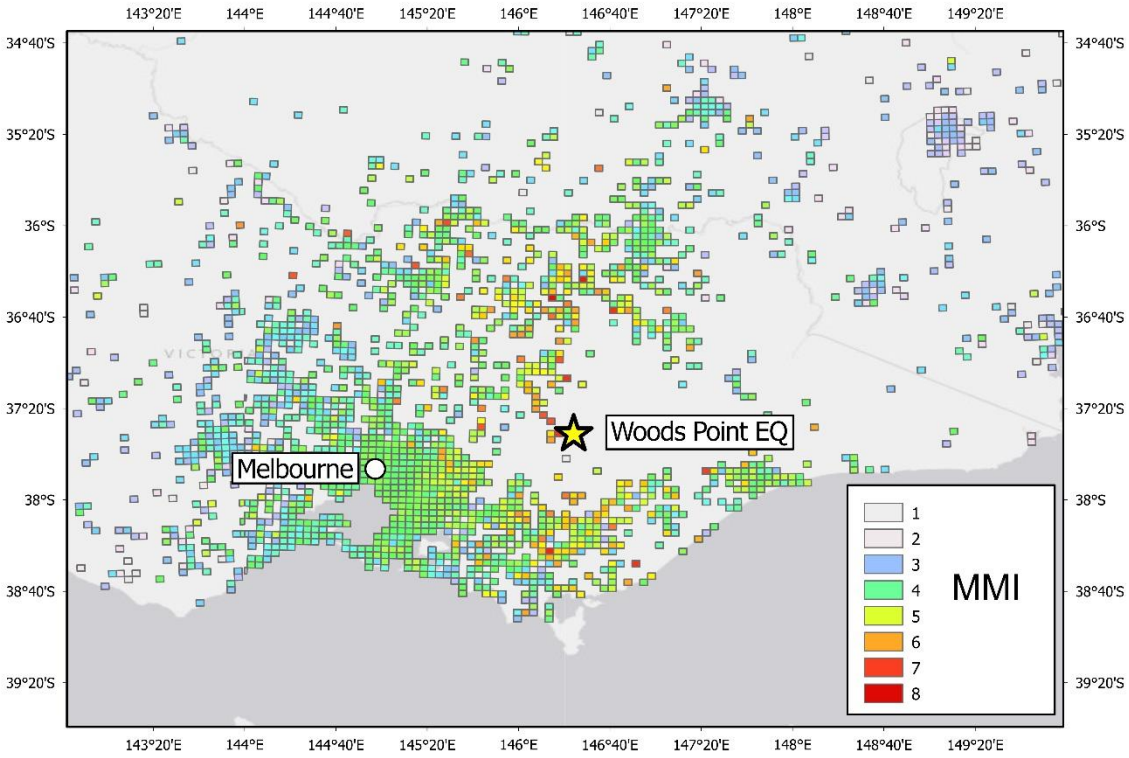

Figure 6: DYFI Felt Grid with 5km spacing of southeast Australia collated by Geoscience Australia. There is a lack of near source data points for the Woods Point earthquake due to lack of population density in the region.

4 Discussion

4.1 Environmental seismic intensity of the Woods Point earthquake

The ESI-07 scale has been used as a tool to assess epicentral seismic intensities and the estimation of epicentral locations of historical earthquakes (Papathanassiou et al., 2017; Rodríguez-Pascua et al., 2017; Ferrario et al., 2022). Ferrario et al., 2022 has published empirical regressions for epicentral intensity as measured by ESI, with M_w. While we do not observe any primary EEEs, we attribute the maximum ESI-07 observed (7) resultant from the WP earthquake as the epicentral intensity. ESI-07 empirical regressions calculate the mean ESI-07 epicentral intensity for a Mw 5.9 strike-slip event as 8.49 (Ferrario et al., 2022) (Figure 7). The WP earthquake ESI epicentral intensity is lower than the mean regression by 1.49 units but still plots within the regression uncertainty.

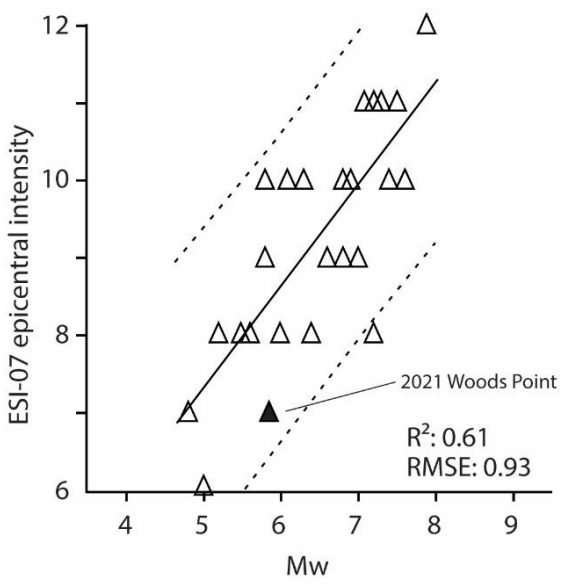

Figure 7: ESI-07 epicentral intensity regression with moment magnitude for global strike slip earthquakes (Ferrario et al., 2022). Modified to include the 2021 Mw 5.9 Woods Point earthquake.

4.2 Lack of near-source intense ground shaking

This lower epicentral shaking intensity when compared with global regressions, including the observation of lack of environmental damage in immediate near-source regions, suggests that shaking intensity in the near-source region of the WP earthquake may be lower than expected for an earthquake of this magnitude and depth. ESI-07 values are lower than predicted MMI values from GMMs, and when compared with MMI DYFI felt reports from moderate epicentral distances (30 – 50kms), the maximum ESI-07 value in the near-source region is consistent with maximum MMI values. The observed pattern of regional azimuthal amplification may influence the near-source region, and this effect on our sample selection could contribute to the apparent lack of near-source shaking intensity.

4.3 Potential mechanisms for lack of near-source shaking intensity

We hypothesise and discuss the possibility for multiple mechanisms to result in lower-than-expected ground motions in the near-source epicentral region for the WP earthquake.

i) Earthquake ruptures commonly exhibit complexity and variability in co-seismic slip magnitudes and vectors, which combines with ray-path and site effect complexities to create large variations in ground motion intensities. Where instrumental ground motion data is not available, anticipated ground motions at a site are subject to large epistemic and aleatoric uncertainty. It may be a result that the WP earthquake near-source ground motions were lower than expected due to aleatoric variability.

ii) Shear wave radiation patterns can amplify and/or dampen ground motions (particularly Spectral Accelerations (SAs) at longer wavelengths) (Kotha et al., 2020) and may have had an effect on the WP earthquake. Primary, Love and Rayleigh waves also exhibit different azimuthal dependency radiation patterns conditional on earthquake frequency (Rösler and van der Lee, 2020). These radiation patterns may have an effect of environmental failure (which may be frequency dependent) through variability in shaking intensity. The inability to collect equally spaced and full azimuthal coverage of EEEs observations around the epicentre/fault rupture adds epistemic uncertainty to the analysis, and difficulty in quantifying a near source azimuthal effect. However, we observe azimuthal

variability of MMI regionally and variability in ESI-07 macroseismic intensity in the near-source region.

iii) Rupture directivity and/or pulse-like/fling effects can also result in asymmetric ground motions within the epicentral region of the earthquake rupture (Hisada and Tanaka, 2021; Vyas et al., 2016). Fling effect has potentially been observed to displace environmental phenomena for the Petermann earthquake (King et al., 2020) and affect ground motion intensity in other strike slip earthquakes (e.g., Imperial Valley earthquake in California; Luo et al., 2020). The Imperial Valley earthquake has shown that as a result of pulse like ground motions, the most intense ground motions were not at the direct epicentral region (Luo et al., 2020). Multicycle simulations of strike-slip earthquake ruptures have also shown that high PGV variability occurs within 20 km R_{jb} distance (Vyas et al., 2016). These effects may be a possible factor for more intense ground motions away from the earthquake epicentre, and towards other sections of the rupture.

5 Conclusions

This work continues to highlight the challenges of ascertaining strong ground motion records close to earthquake epicentres. This study documents and analyses EEEs with the macro seismic intensity scale - ESI-07, to attempt to understand the distribution of ground motion (given the lack of instrumental data) in the Woods Point epicentral region. We observe a lower-than-expected ESI-07 binned mean intensities when compared with the MMI converted from SGC09 GMM PGV, and lower epicentral intensities when compared with regression of other strike slip earthquakes documented with the ESI-07 scale. Earthquakes are aleatoric in nature, and multiple mechanisms including rupture directivity, radiation patterns, and fling/pulse like ground motions, may have impacted the distribution of macroseismic intensity from the Woods Point earthquake.

6 References

Aagaard, B. T., Hall, J. F., & Heaton, T. H. (2004). Effects of fault dip and slip rake angles on near-source ground motions: Why rupture directivity was minimal in the 1999 Chi-Chi, Taiwan, earthquake. Bulletin of the Seismological Society of America, 94(1), 155-170.

Allen T (2012) Stochastic Ground-motion Prediction Equations for southeastern Australian Earthquakes using Updated Source and Attenuation Parameters (Record 2012/69). Canberra, ACT, Australia: Geoscience Australia.

Atkinson, G. M., & Kaka, S. I. (2007). Relationships between felt intensity and instrumental ground motion in the central United States and California. Bulletin of the Seismological Society of America, 97(2), 497-510.

Atkinson, G. M., Worden, C. B., & Wald, D. J. (2014). Intensity prediction equations for North America. Bulletin of the Seismological Society of America, 104(6), 3084-3093.

Dreger, D., Hurtado, G., Chopra, A., & Larsen, S. (2011). Near-field across-fault seismic ground motions. Bulletin of the Seismological Society of America, 101(1), 202-221.

Galvez, P., Petukhin, A., Somerville, P., Ampuero, J. P., Miyakoshi, K., Peter, D., & Irikura, K. (2021). Multicycle simulation of strike-slip earthquake rupture for use in near-source ground-motion simulations. Bulletin of the Seismological Society of America, 111(5), 2463-2485.

Hisada, Y., & Tanaka, S. (2021). What is fling step? Its theory, simulation method, and applications to strong ground motion near surface fault ruptures. Bulletin of the Seismological Society of America, 111(5), 2486-2506.

Hoult, R. D., Pascale, A., Jones, A., & Allen, T. (2021, November). The MW 5.9 Woods Point earthquake: A preliminary investigation of the ground motion observations. In Proceedings of the Australian Earthquake Engineering Society 2021 Conference, Virtual (pp. 25-26).

Huang, Y., Quigley, M., La Greca, J., Wilcox, J,. Borleis, E., Peck, W. (2024). Statistical properties and modelled duration of an intracontinental earthquake sequence: 2021 Mw 5.9 Woods Point earthquake, Australia. In Proceedings of the Australian Earthquake Engineering Society 2024, Adelaide

King, T., Quigley, M., & Clark, D. (2020). Near-field directionality of earthquake strong ground motions measured by displaced geological objects (No. EGU2020-12092). Copernicus Meetings.

Kotha, S. R., Cotton, F., & Bindi, D. (2019). Empirical models of shear-wave radiation pattern derived from large datasets of ground-shaking observations. Scientific reports, 9(1), 981.

La Greca, J., Quigley, M., Vaculik, J., Rayner, P., & Allen, T. (2024). Bayesian analysis of ground motion models using chimney fragility curves: 2021, 5.9-Mw Woods Point intraplate earthquake, Victoria, Australia. Earthquake Spectra, 40(1), 732-759.

Leonard, M. (2015, November). Consistent MMI area estimation for Australian earthquakes. In Proceedings of the Tenth Pacific Conference on Earthquake Engineering Building an Earthquake-Resilient Pacific (p. 9).

Luo, Q., Dai, F., Liu, Y., & Chen, X. (2020). Simulating the near-field pulse-like ground motions of the Imperial Valley, California, earthquake. Soil Dynamics and Earthquake Engineering, 138, 106347.

Luo, Q., Dai, F., Liu, Y., & Chen, X. (2020). Simulating the near-field pulse-like ground motions of the Imperial Valley, California, earthquake. Soil Dynamics and Earthquake Engineering, 138, 106347.

Michetti, A. M., Guerrieri, L., & Vittori, E. (2007). Intensity scale ESI 2007. SystemCart.

Mousavi, S., Hejrani, B., Miller, M. S., & Salmon, M. (2023). Hypocenter, fault plane, and rupture characterization of Australian earthquakes: application to the September 2021 M w 5.9 woods point earthquake. Seismological Society of America, 94(4), 1761-1774.

Rösler, B., and S. van der Lee (2020). Using Seismic SourceParameters to Model Frequency-Dependent Surface-Wave Radiation Patterns, Seismol. Res. Lett. 91, 992–1002, https://doi.org/10.1785/0220190128.

Serva, L. (2019). History of the Environmental Seismic Intensity Scale ESI-07. Geosciences, 9(5), 210.

Somerville, P. G., Smith, N. F., Graves, R. W., & Abrahamson, N. A. (1997). Modification of empirical strong ground motion attenuation relations to include the amplitude and duration effects of rupture directivity. Seismological research letters, 68(1), 199-222.

Tang, Y. (2022a). An Updated Corner-frequency Model for Stochastic Finite-fault Ground Motion Simulation. Bulletin of Seismological Society of America, 112 (2): 921-938.

Tang, Y. (2022b). GMSS2. 0: An Enhanced Software Program for Stochastic Finite-Fault Ground-Motion Simulation. Seismological Research Letters, 93(3), 1868-1879.

Tang, Y., & Martin Mai, P. (2023). Stochastic Ground-Motion Simulation of the 2021 M w 5.9 Woods Point Earthquake: Facilitating Local Probabilistic Seismic Hazard Analysis in Australia. Bulletin of the Seismological Society of America, 113(5), 2119-2143.

Vyas, J. C., Mai, P. M., & Galis, M. (2016). Distance and azimuthal dependence of ground-motion variability for unilateral strike-slip ruptures. Bulletin of the Seismological Society of America, 106(4), 1584-1599.

Wood, H. O., and Neumann, Frank (1931). Modified Mercalli Intensity Scale of 1931: Seismological Society of America Bulletin, v. 21, no. 4, p. 277-283.